Buried Pd slows self-diffusion on Cu(001)

E. Bussmann,[1,*] I. Ermanoski,[1] P. J. Feibelman,[1] N. C. Bartelt,[2] and G. L. Kellogg[1]
[1]*Sandia National Laboratories, Albuquerque, New Mexico 87185, USA*
[2]*Sandia National Laboratories, Livermore, California 94551, USA*
(Received 11 January 2011; revised manuscript received 14 November 2011; published 21 December 2011)

Using low-energy electron microscopy, we determine that self-diffusion of the Cu(001) surface is slowed by the presence of a $c(2 \times 2)$-Pd buried surface alloy. We probe surface diffusion using Cu-adatom island-ripening measurements. On alloyed surfaces, the island decay rate decreases monotonically as the Pd concentration is increased up to ∼0.5 monolayer (ML), where the 2×2 buried alloy is Pd saturated. We propose that the Pd slows island ripening by inhibiting the diffusion of surface vacancies across terraces. For dilute alloys ($\lesssim$0.2-ML Pd), this conclusion is supported by density-functional theory calculations, which show that surface vacancies migrate more slowly owing to an attraction to isolated buried Pd atoms. The results illustrate a fundamental mechanism by which even a dilute alloy thin-film coating may act to inhibit surface-diffusion-mediated processes, such as electromigration.

DOI: 10.1103/PhysRevB.84.245440 PACS number(s): 68.35.bd, 68.35.Fx, 68.37.Nq, 68.60.Dv

I. INTRODUCTION

Surface self-diffusion, by which a surface attains its thermodynamic equilibrium structure, is fundamental in processes such as epitaxy.[1] For example, 2D adatom islands nucleated during layer-by-layer epitaxial growth are prone to Ostwald ripening, via diffusion of mass between islands, which minimizes the excess free energy associated with the atomic step edges surrounding the islands.[1–5] A small fraction of a monolayer (ML) of foreign atoms in or on a surface can change surface diffusion rates significantly.[5–8] On Cu(111) surfaces, just 0.01 ML of adsorbed sulfur enhances surface diffusion by several orders of magnitude.[6] By contrast, Anderson *et al.* found that lead atoms embedded in the Cu(111) surface suppress diffusion rates by several orders of magnitude—the surface diffusion barrier increases from 0.8 to 0.9 eV with 0.11-ML Pb and to 1.2 eV with 0.22-ML Pb.[5] Surface diffusion is slowed because surface-embedded Pb atoms increase the barrier to Cu adatom diffusion across terraces. A similar mechanism has been proposed for the inhibition of Cu adatom diffusion on Cu-Sn alloy surfaces.[9]

In the Cu(001)-$c(2\times2)$-Pd buried surface alloy system, the Pd alloy is covered by a nearly pure layer of copper.[10–15] It is not evident that the buried Pd will have a significant influence on surface mass transport. In this work, we use Cu-adatom island-ripening measurements to show that Cu(001) surface diffusion is slowed by the presence of buried Pd atoms near the surface. Previous studies[3,4,16–18] found that Cu(001) surface diffusion is mediated by surface vacancies, and we propose that the alloy slows surface diffusion by increasing the energetic barrier to vacancy diffusion. Using first-principles density-functional theory calculations, we find that Cu surface vacancies are attracted to buried Pd atoms, which inhibits vacancy migration on alloyed terraces.

Surface self-diffusion also determines how fast a surface is reorganized under externally imposed driving forces. For example, electromigration in thin ($<$0.15 μm) Cu microelectronic wires is a surface-diffusion-limited process.[7] Bulk alloying is a proposed means to harden Cu wires against damaging electromigration effects.[19] Previous studies have found that Pd-Cu bulk alloy films are less susceptible than pure Cu films to electromigration damage: the electromigration activation barrier, 0.8 eV for Cu, increases to 1.01 eV with 0.5 wt% Pd and 1.2 eV for 1.26 wt% Pd.[8] Since electromigration in thin wires is surface diffusion limited, the results we present here suggest that electromigration in a Cu thin film can be slowed by a Pd-Cu surface alloy coating. Chen *et al.*[9] predict that Cu-Sn surface alloying may also serve to inhibit Cu electromigration.

II. EXPERIMENT

A. Methods and materials

Our experiments are done in an ELMITEC LEEM III at pressures below 5×10^{-10} Torr. We use a single-crystal Cu (99.999%) sample cut and electropolished to within ∼0.1° of the [001] orientation. Prior to experiments, the sample is annealed in a furnace at 900 °C in an atmosphere of Ar4%H_2 for 24 h to deplete sulfur and carbon contamination. The sample surface is prepared by numerous cycles of 1-keV Ar or Ne ion sputtering and then annealed at 700–800 °C. When the sample is sufficiently clean that a step-terrace surface structure is visible in LEEM images, the sample is further prepared by sublimation (850 °C) of several atomic layers of Cu. The flow of monatomic surface steps during sublimation is observed by LEEM. Residual contaminant particles (oxides, sulfur, and carbon) too small to be resolved by LEEM can be identified because they impede step flow during sublimation. We perform the island decay experiments on terraces that exhibit smooth unimpeded step flow during sublimation.

We prepare the Cu(001)-$c(2 \times 2)$-Pd buried surface alloy by depositing Pd (5 ML/h) from an *e*-beam-heated wire source onto the sample held at 210 °C. The structure, and growth, of the $c(2 \times 2)$-Pd alloy are well understood.[10–15,20] The buried alloy forms when submonolayer coverages of Pd are deposited on Cu(001) at $T > 150$ °C. On terraces, Fig. 1(a), the alloy consists of a $c(2 \times 2)$-ordered Pd-Cu underlayer covered by a relatively pure layer of Cu.[13] Near step edges, some Pd is also present in the third atomic layer, as shown in Fig. 1(b). Hannon *et al.* showed that this structure originates from step flow during the growth of the alloy.[14] As Pd adsorbed on

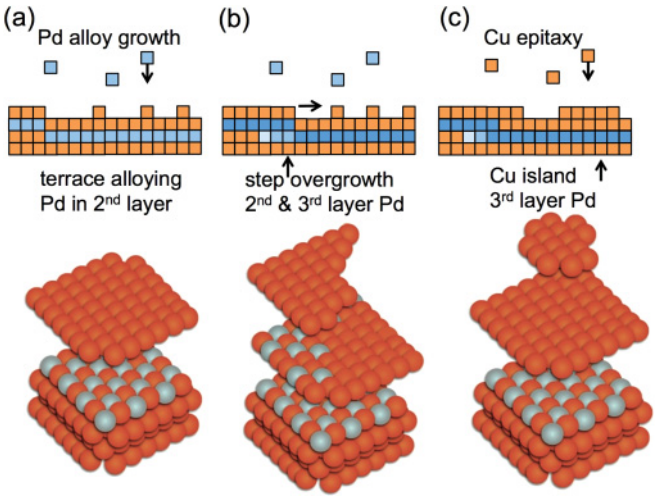

FIG. 1. (Color online) Schematic representation of the growth and composition of the $c(2 \times 2)$-Pd buried surface alloy

the terrace is incorporated into the second atomic layer, Cu is displaced to the surface. The displaced Cu migrates to nearby steps, causing the steps to advance. The advancing steps grow over the alloy on the terrace, burying Pd in the third atomic layer; see Fig. 1(b). On the upper side of the step, arriving Pd continues to be incorporated into the second layer as well, leading to Pd in both the second and third layers. On clean and alloyed surfaces, Cu adatom islands are grown by Cu deposition (~2 ML/min) from an *e*-beam-heated Cu (99.999%) ingot. During the Cu deposition, the temperature of the sample is 210 °C. The islands develop shapes similar to the published equilibrium shape for the Cu(001) surface.[21] Examples of adatom islands on the clean and alloy surfaces are shown in several figures, e.g., Figs. 2 and 3.

B. LEEM characterization of the surface alloy

Prior to an island-ripening experiment, we use LEEM intensity-versus-voltage (*I-V*) measurements to verify that the surface alloy has the structure shown in Fig. 1.[14,15] In an *I-V* measurement, specular LEEM images are recorded versus the energy of the incident electrons. The energy-dependent electron reflectivity is sensitive to the surface structure to a depth of several atomic layers.[14,15] LEEM *I-V* measurements can reveal inhomogeneity, e.g., spatial variations in Pd concentration, or compositional changes at the surface during island-ripening measurements.[14,15,22]

Figure 2 shows images of the surface alloy (0.4-ML Pd) with epitaxial Cu adatom islands. Structural and compositional variations in the alloy produce the contrast in the images. Two recent publications explain the cause of the contrast.[14,15] At 14.5 eV, Fig. 2(a), the terrace regions, with second-layer Pd, appear dark. Brighter regions contain some Pd in the third atomic layer, as near terrace edges, and under Cu islands; see Fig. 1(c).

The small roughly circular bright spots are Cu adatom islands. The other larger bright regions with nonuniform shapes are monolayer-high Cu structures created by step flow growth or island coalescence during Cu deposition. At 20.5 eV, Fig. 2(b), the 14.5-eV contrast is reversed. Figure 2(c) is

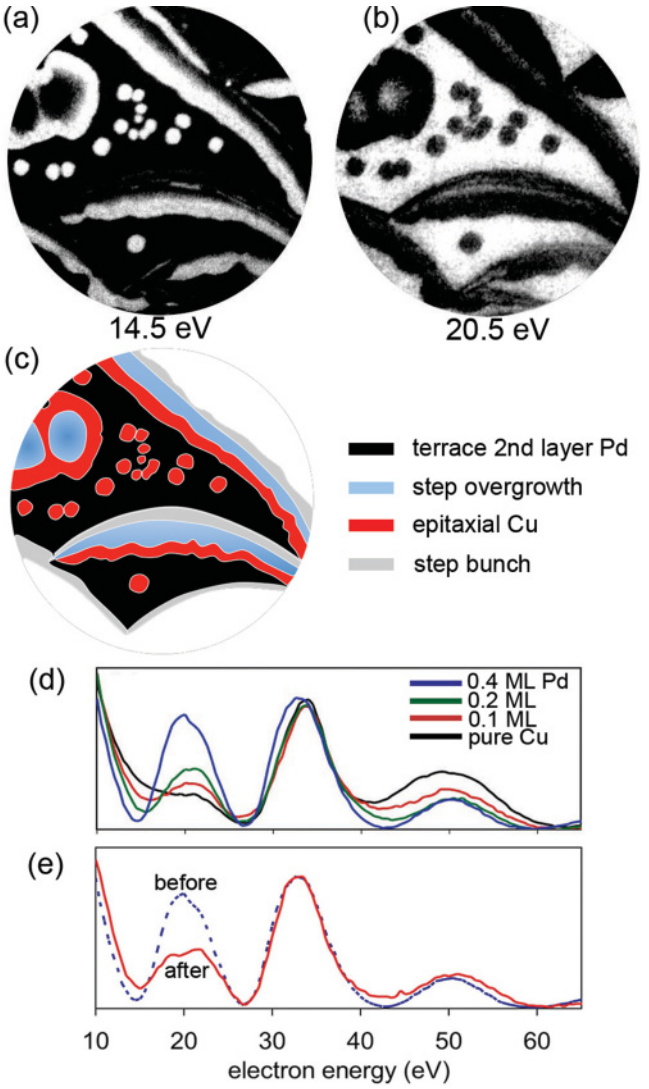

FIG. 2. (Color online) LEEM characterization of $c(2 \times 2)$-Pd buried surface alloy. The image contrast is sensitive to the surface composition and the electron energy, (a) 14.5 eV and (b) 20.5 eV (0.4 ± 0.05-ML Pd, field of view $= 3\ \mu$m). (c) A schematic drawing identifying various structures on the surface. (d) Intensity-versus-electron energy (I-V) curves on terraces of the Pd-Cu alloy structure for pure Cu and 0.1-, 0.2-, and 0.4-ML Pd concentrations. The peak at ~20.5 eV grows nearly in proportion to the Pd concentration. (e) I-V measurements before and after annealing a 0.4-ML Pd alloy. Pd diffusion into the bulk is tracked by I-V measurements. After annealing (1.5 h, 240 °C), the double-peak near 20 eV indicates significant Pd in the fourth layer below the surface.

a drawing showing the locations of the structures described in Fig. 1.

By recording the intensity as a function of the electron energy at given location on the sample, one obtains an *I-V* curve, Figs. 2(d) and 2(e). Recent studies have extensively catalogued the characteristics of the *I-V* curves for the $c(2 \times 2)$-Pd surface as a function of Pd coverage. As with low-energy electron diffraction (LEED) *I-V* measurements, the *I-V* relationship can be fit by a multiple-scattering LEED calculation by optimizing a trial surface structure.[23] This technique was applied by Hannon *et al.* to reveal the

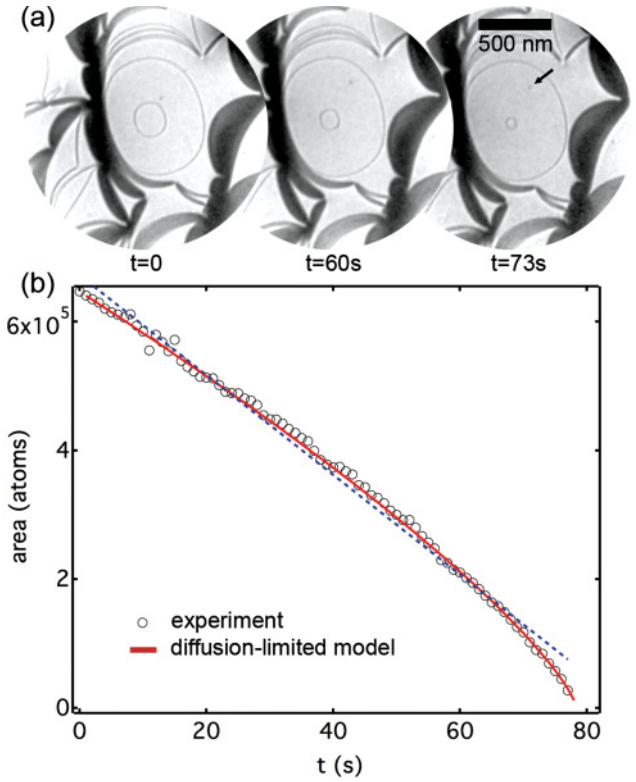

FIG. 3. (Color online) Decay of a small island isolated on top of a larger island ($T = 310\,^{\circ}$C, e^{-}energy $= 2$ eV). (a) LEEM images of the island decay. An arrow points to a defect on the microchannel plate in the imaging system. (b) Area versus time of the small island. The broken blue line is a line fit to the experimental data, shown to emphasize that the island decay in the experiments is nonlinear.

step-overgrowth mechanism that produces the step edge structure shown in Fig. 1(b). We use LEEM *I-V* measurements as a fingerprinting technique, utilizing the extensive published LEEM *I-V* curves and calculated structures for the $c(2 \times 2)$-Pd surface as a reference.[14,15,22] Figure 2(d) shows LEEM *I-V* curves from a clean Cu terrace and terraces with the alloy structure of Fig. 1(a) with concentrations of 0.1-, 0.2-, and 0.4 ± 0.05-ML Pd. As shown in recent publications, the peak at $\sim$20.5 eV in the curves grows nearly in proportion to the Pd concentration ($\lesssim$0.5 ML) in the alloyed layer.[14,15,22]

By comparing *I-V* curves before and after each ripening experiment, we can determine whether the surface alloy composition has changed during the experiment. By this method, we have found that thermal instability, by Pd diffusion into the Cu bulk, of the surface alloy puts an upper bound on the temperature range, and duration, for the ripening experiments. Figure 2(e) shows *I-V* curves from an initially 0.4-ML surface alloy before, and after, a ripening measurement (240 °C) of 1.5 h duration. After the ripening measurement, the intensity of the 20-eV peak has dropped, and the *I-V* profile has developed a double peak. Additional experiments, supported by LEEM *I-V* analysis, indicate that the double peak is caused by Pd content within the fourth layer.[22] During the measurements, Pd is diffusing deeper into the surface. This is not surprising, as previous measurements, in the temperature range 800–1100 °C, have determined that the barrier for Pd diffusion into the copper bulk is $\sim$2 eV. Assuming a diffusion activation prefactor of 10^{13} s^{-1}, the expected diffusion length, $2(Dt)^{1/2}$, is 0.5 atomic layers.[24] At lower Pd concentrations (<0.2 ML) the island decay is more than 10 times faster, and at 240 °C, Pd loss to the bulk is not significant over the time scale of the island decay. We have explored the diffusion of Pd into the Cu(001) surface in a recent publication.[22]

III. ANALYSIS OF ISLAND RIPENING

A. The role of diffusion and attachment barriers in island ripening

In this section, we introduce the equations we use to analyze the evolution of island ensembles. Since previous STM work has shown that island ripening on clean Cu(001) can be influenced by a barrier to attachment of surface vacancies at step edges, we will review the effect of this barrier on the island ripening and show that when the islands become large and well separated it can be neglected. In the next section, we will show that our LEEM experiments are in this diffusion-limited regime.

Adatom islands raise the total step length, and the free energy, of a surface.[2] During ripening, the surface free energy (excess step length) is minimized: Small islands tend to decay, while larger islands grow. On the clean Cu(001) surface, the ripening process is mediated by currents of vacancies between islands.[3,4] The currents arise from differences in vacancy concentration at the edges of islands with different radii (curvature).

The equilibrium vacancy concentration at the edge of a step with local curvature κ_s is given by the Gibbs-Thomson relation, $c = c^{\infty} \exp(-\tilde{\beta}\kappa_s a^2/k_B T)$.[2] Here, c^{∞} is the concentration in equilibrium with a straight step, $\tilde{\beta}$ is the step stiffness, and a^2 is the area associated with an adatom in the island. To analyze our island-ripening data, we use a model with circular islands, i.e., isotropic step stiffness, in a cylindrical geometry.[2] We justify this assumption by the fact that we observed no significant changes in the roughly circular island shapes with changing Pd concentration, or temperature, in our experiments. Thus, it is unnecessary to specify the local step curvatures and the Gibb-Thomson equilibrium concentration at an island edge is simply determined by its average radius R: $c = c^{\infty} \exp(-\beta a^2/Rk_B T)$, where β is the line tension of the step edge.[2] Predicting the area-versus-time relationship for an island is done by solving the diffusion equation between islands using the Gibbs-Thomson relation to establish the boundary concentration at each step.

To get insight into the kinetics of island decay, we have measured the decay of epitaxial island stacks, and individual isolated islands on terraces; see Fig. 3. To model island decay in this arrangement, we approximate the geometry using a single (circular) adatom island of radius R_1, located at the center of a larger island (terrace) of radius R_2. In this model the area, A_1, of the upper island decreases at a rate[2]

$$\frac{dA_1}{dt} = -\frac{2\pi a^4 \beta D c^{\infty}}{k_B T} \frac{(1/R_1 - 1/R_2)}{\ln(R_2/R_1) + a/\kappa R_1}, \qquad (1)$$

where D is the hopping rate of the mass-carrying species (vacancies) and κ is the ratio of the vacancy attachment rate at step edges relative to the vacancy hop rate on the terrace.

Two limiting cases of this formula are relevant in our ripening measurements. If the attachment rate, κ, of mass-carrying species is sufficiently small that $a/\kappa R_1 > \ln(R_2/R_1)$, the decay is attachment limited and

$$\frac{dA_1}{dt} = -\frac{2\pi a^3 \beta \kappa D c^{\infty}}{k_B T} R_1 (1/R_1 - 1/R_2). \quad (2)$$

The rate approaches a constant when $R_1 \ll R_2$. In their STM study, Hannon *et al.* measured island decay on Cu(001) described accurately by attachment-limited kinetics.[3,4] In a system with an attachment barrier, attachment-limited kinetics gives way to diffusion-limited kinetics if the length scale (R_1, R_2) involved in the measurement is sufficiently large that $a/\kappa R_1 < \ln(R_2/R_1)$. In strictly diffusion-limited kinetics,

$$\frac{dA_1}{dt} = -\frac{2\pi a^4 \beta D c^{\infty}}{k_B T} \frac{(1/R_1 - 1/R_2)}{\ln(R_2/R_1)}. \quad (3)$$

Here, when the islands are small, $R_1 \ll R_2$, the decay is not linear but instead $A \propto t^{2/3}$. As we discuss in the next section, island decay in our measurements is in the diffusion-limited regime, in contrast to the attachment-limited kinetics of Hannon *et al.*'s lower-temperature, smaller-scale STM study.

Unfortunately, one cannot use Eq. (3) to analyze the ripening of ensembles of islands, see Fig. 2(a), which are typically found on each terrace after Cu deposition. In this case, mass is exchanged among the islands, as well as with nearby step edges. A phenomenological model developed to analyze this situation is given in the review of Zinke-Allmang *et al.*.[25] In this model, the time dependence of an ensemble of islands of area A_i is

$$\frac{dA_i}{dt} = -\frac{2\pi a^4 \beta D c^{\infty}}{k_B T} \frac{(1/R_i - 1/R_c)}{\ln(l_i) + a/\kappa R_i}, \quad (4)$$

where R_i is the radius of island i. The length l_i specifies the distance over which the concentration decays to its value far from the step edge. We use l_i as a (fitting) constant. The value of R_c determines whether a given island grows or shrinks, i.e., islands with $R_i > R_c$ grow while islands with $R_i < R_c$ shrink. Typically, $R_c(t)$ is of the same order of magnitude as the mean radius of the islands in the ensemble, and the value is determined by global mass conservation.[3] Analogous to Eq. (1), ripening of an ensemble can be either attachment or diffusion limited, cf. Eqs. (2) and (3), depending on whether $\ln(l_i)$ or $a/\kappa R_i$ is greater.

Recall, $Dc^{\infty} \propto \exp(-E_m/k_B T)$ and $c \propto \exp(-E_f/k_B T)$, where E_m is the barrier to diffusive hopping and E_f is the formation energy of the mass-carrying species. In the diffusion-limited regime, the activation barrier for island ripening is $E_a = E_f + E_m$, while in attachment-limited ripening, $E_a = E_f + E_s$, where E_s is the barrier to attachment of the mass-carrying species to a step edge.

B. Island-ripening measurements

1. Clean Cu(001)

In an island-ripening measurement, the sample is heated to a fixed temperature (150–350 °C). A sequence of LEEM images, acquired at fixed time intervals, is recorded to form a movie of the ripening process. The area of each island is measured in every image by an automated edge-marking program. Figures 3 and 4 show images of the ripening process, and the corresponding area versus time measurements, for islands on the clean Cu surface.

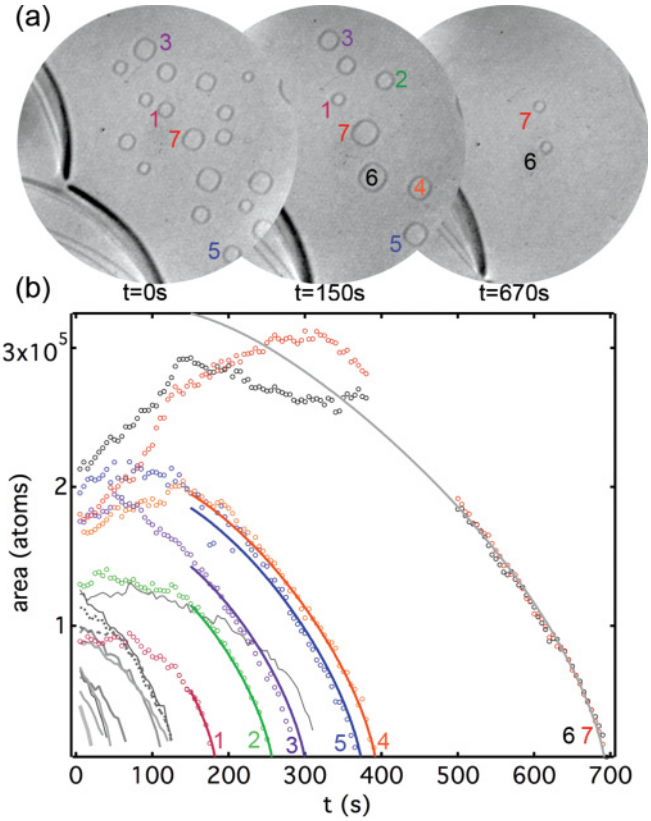

FIG. 4. (Color online) (a) Ripening of a group of islands on the pure Cu(001) surface at $T = 240\,^{\circ}$C (field of view = 1.6 μm, e^-energy = 2 eV). (b) The area-versus-time relationships for all the islands along with the prediction of Eq. (4). Note that larger islands grow in direct response to the decay of relatively smaller islands in the neighborhood.

We begin by exploring the decay of individual adatom islands near the centers of larger terraces, as shown in Fig. 3(a). For isolated islands on large terraces, we do not observe the linear decay, Fig. 3(b), predicted by attachment-limited kinetics [Eq. (2)] and measured previously by Hannon *et al.*.[3,4] Instead, diffusion-limited kinetics [Eq. (3)] accurately fits the area-versus-time relationship. The fitting parameter is the surface self-diffusion coefficient $Dc^{\infty} = 1.81 \times 10^5\ \mathrm{s}^{-1}$ ($T = 310\,^{\circ}$C). To fit, we assume a step line tension, $\beta a = 210$ meV.[26]

A crossover from attachment to diffusion-limited kinetics is expected if the size, R_1 and R_2, of the islands and terraces is sufficiently large that $a/\kappa R_1 \ll \ln(R_2/R_1)$. Hannon *et al.*'s STM measurements involved much smaller islands and terraces, about 1/10 of the sizes in our measurements. In our measurements, where $a/R_1 \sim 1000$ and $\ln(R_2/R_1) \sim 1$, strictly attachment-limited kinetics would require that $\kappa \lesssim 10^{-4}$.

Over the temperature range of our experiments, diffusion-limited kinetics accurately fits the decay of isolated islands. Figure 5(a) shows decay curves for isolated islands, at several temperatures, with fits using Dc^{∞} as the fit parameter. The values of Dc^{∞} are plotted in Fig. 5(b). A fit to the data yields $Dc^{\infty} = 10^{12.5\pm0.5} \exp(-0.83 \pm 0.03\ \mathrm{eV}/k_B T)\ \mathrm{s}^{-1}$.

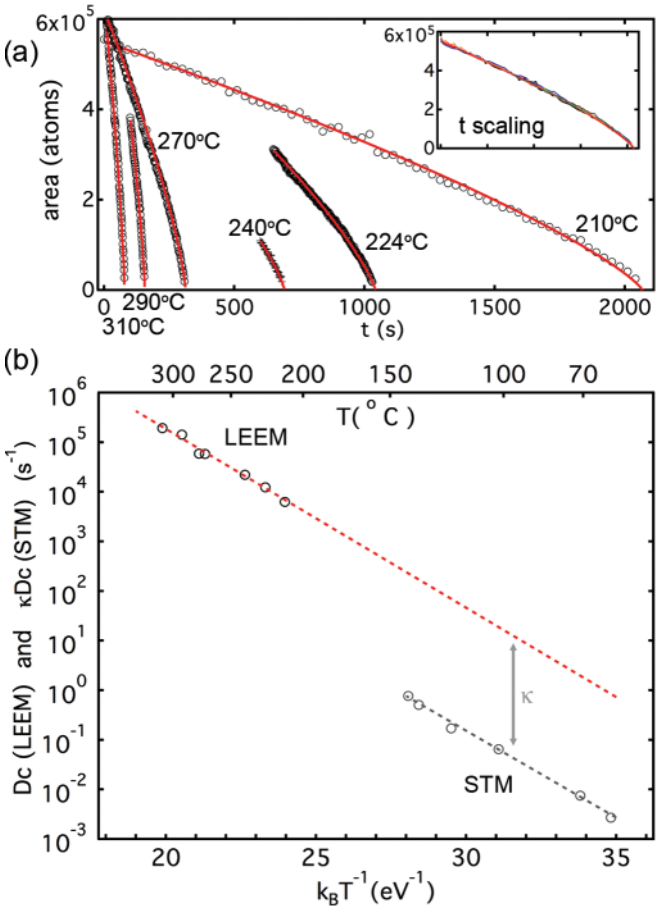

FIG. 5. (Color online) (a) Decay of isolated islands at various temperatures. The red solid curves are fits by the diffusion-limited model. (b) Temperature dependence of Dc^{∞} determined by fitting island decay measurements. The values of κDc^{∞} are calculated from island decay rates given in Ref. 4. Note that Dc^{∞} has been shortened simply to Dc on the vertical axis.

The inset in Fig. 5(a) shows all the decay curves with the time scaled so the curves fall on top of one another. By fitting the time-scaling factors in Arrhenius form, we get a second measurement of the activation barrier for island decay, 0.9 ± 0.1 eV, that is in reasonable agreement with the first result (0.83 eV).

Figure 5(b) also shows values of κDc^{∞} that we have calculated, via Eq. (2), from the attachment-limited island decay rates in Refs. 3 and 4. The offset between our data (Dc^{∞}) and the values of κDc^{∞} is $\kappa \simeq 1/300$. Recall that attachment-limited kinetics at the length scales of our measurements requires $\kappa < 10^{-4}$. Therefore, it is not surprising that we find diffusion-limited kinetics. However, it is surprising that we find an identical activation barrier (~0.8 eV) for island decay, meaning that attachment-limited kinetics does not arise from an additional barrier to attachment but rather from a lower attempt frequency for step edge attachment than for hopping.

Individual islands isolated on terraces are a special case. More often, we find small ensembles of islands on a terrace. Figure 4 shows the ripening of a small group of islands on the pure Cu surface. Characteristic of diffusion-limited ripening, we observe "neighborhood effects": as small islands decay and vanish, relatively larger neighboring islands (e.g., islands 6 and 7) tend to grow in direct response.

Taking the diffusion limit, $\ln(R_2/R_1) \gg a/\kappa R_1$ in Eq. (4), we can predict the evolution of the island ensemble. Equation (4) does not account for direct neighborhood effects; nevertheless, it can be used to make a qualitative approximation to the the evolution of the ensemble. The fit yields two parameters, $Dc^{\infty}/\ln(l_i) = 1800\ \mathrm{s}^{-1}$, and the initial value of $R_c(t)$ equal to 1.7 times the mean island radius. The fit serves only to show that the evolution of the ensemble is in reasonable qualitative agreement with the predictions of diffusion-limited ripening. We start the fit from $t = 150$ s, since the model cannot account for the neighborhood effects between the smaller dense islands at $t = 0$ s.

2. *Pd alloy surfaces*

Having determined that on clean Cu surfaces ripening is diffusion limited on the length scales of our experiment, we are in a position to determine if the effect of added Pd is to change an attachment barrier at the step edge or to change a diffusion barrier. We will show that on Pd alloy surfaces, island ripening is also diffusion limited so Pd changes the barrier to diffusion on the terraces.

Figures 6 and 7 show ripening on alloy surfaces. The decay ($T = 230\,^{\circ}$C) of a single isolated island on a terrace with 0.06 ± 0.03-ML Pd alloy is shown in Fig. 6 along with a fit by the diffusion-limited model, Eq. (3). The best-fit value of

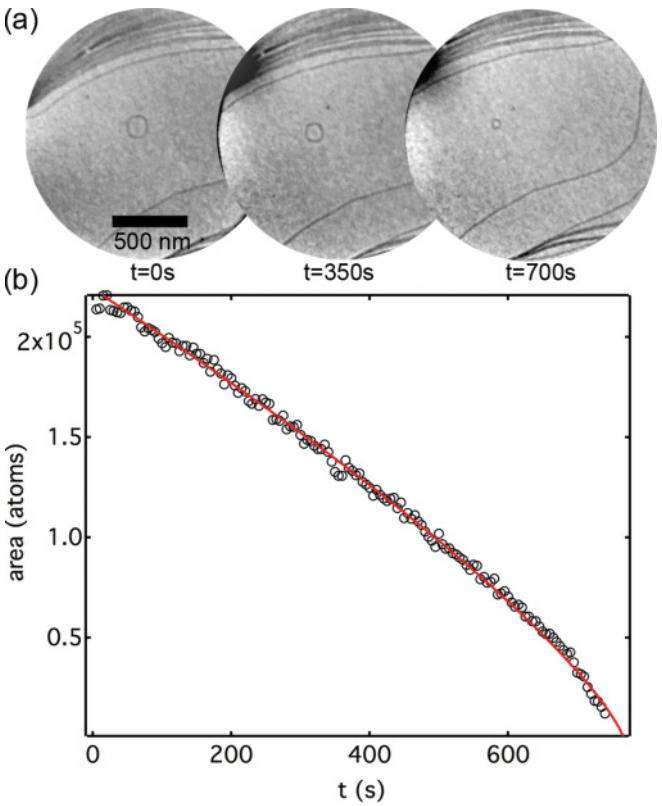

FIG. 6. (Color online) Decay of an isolated island on the 0.06 ± 0.03-ML Pd alloy surface is in the diffusion-limited regime of Eq. (2) ($T = 230\,^{\circ}$C, field of view = 1.6 μm, e^{-}energy = 2 eV).

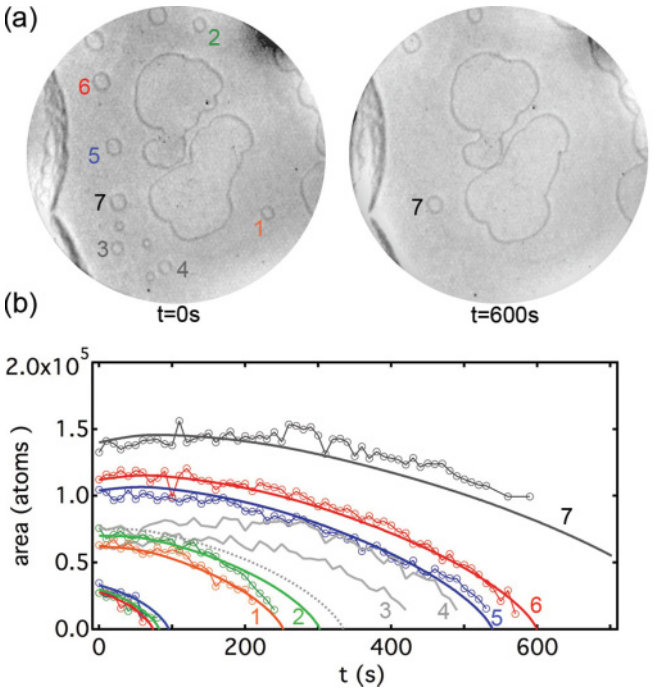

FIG. 7. (Color online) Ripening of a small island group on the 0.2-ML Pd alloy surface at $T = 240\,^{\circ}$C with fits by Eq. (4). The gray dotted line shows the calculated evolution of islands 3 and 4 (field of view = 1.6 μm, e^{-}energy = 2 eV).

Dc^{∞} is 5700 s^{-1}, which is less than half of the value of Dc^{∞} (14 400 s^{-1}) for the pure Cu surface.

Figure 7 shows the ripening of small groups of islands at 240 °C on a 0.2-ML Pd alloy. We consider only the decay of the smaller (numbered) islands. The much larger irregular shaped Cu islands at the center of Fig. 7 are formed when groups of islands coalesce during growth. Figure 7(b) shows fits to the area-versus-time curves predicted by Eq. (4) in the diffusion limit. Diffusion-limited kinetics provides a reasonable fit to the behavior. Neighborhood effects are again evident. For example, islands 3 and 4 grow in response to the decay of smaller neighboring islands and vanish later than similar isolated islands 1 and 2. Equation (4) does not account for neighborhood effects and, hence, does not fit the ripening of islands 3 and 4. Comparing Fig. 7 with Fig. 4, which shows data for the pure Cu surface, it is clear that island decay is slower on the alloy, for example, islands with $\sim 10^5$ atoms decay in less than 200 s on the pure surface, as compared to 500–600 s on the alloyed surface.

The diffusion-slowing effect of the Pd alloy is made clear by measuring the island decay rates versus the Pd concentration at a fixed temperature. Figure 8(a) shows how the value of Dc^{∞} determined by fitting island decay rates depends on Pd concentration at $T = 240\,^{\circ}$C. Values of Dc^{∞} decrease monotonically with increasing Pd concentration. With ~0.4-ML Pd, Dc^{∞} is reduced by more than an order of magnitude.

The buried alloy raises the activation barrier, E_a, for island decay. The value of E_a is determined by an Arrhenius analysis of the temperature dependence of Dc^{∞}. Values of Dc^{∞}, obtained by fitting island decay rates for the clean Cu surface, and a surface with 0.06 ± 0.03-ML Pd buried alloy

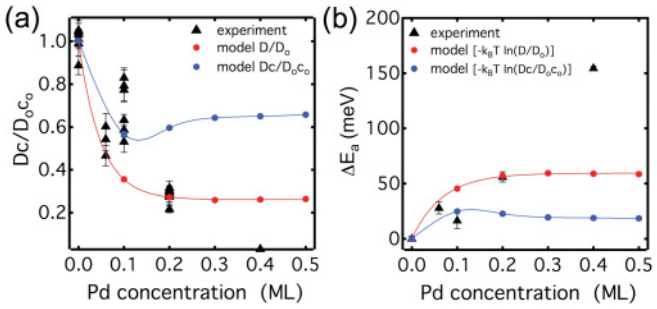

FIG. 8. (Color online) Slowing of island decay with increasing Pd concentration. (a) Dependence of $Dc^{\infty}/D_o c_o^{\infty}$ on Pd coverage at $T = 240\,^{\circ}$C. Here Dc^{∞} is the measured diffusion coefficient, obtained from fits to island-ripening curves, for a given Pd coverage, and $D_o c_o^{\infty}$(=20 000 s^{-1}) is the rate for the clean surface. The solid lines are the results of our KMC simulation. The red line is the calculated value of D/D_o, including only the change in the effective migration barrier and ignoring changes in the vacancy formation energy and concentration c. The blue line is the complete result for $Dc^{\infty}/D_o c_o^{\infty}$, including the Pd-coverage-dependent migration barrier and the formation energy. Note that Dc^{∞} has been shortened simply to Dc on the vertical axis. (b) Estimate of the change in the activation barrier for island decay versus Pd concentration. The solid lines are the results of our Monte Carlo simulations. The red line includes changes in the effective migration barrier and ignores changes of the vacancy formation energy. The blue line is the calculated value of ΔE_a, including changes in the effective migration barrier and formation energy.

are plotted in Arrhenius form in Fig. 9. On the alloyed surface (0.06 ML), the activation barrier for island decay is increased to 0.86 ± 0.07 eV. For higher Pd concentrations, island decay is slowed sufficiently that Pd loss into the bulk on the time scale of the island decay measurements makes it impractical to extract the activation barrier by a complete Arrhenius

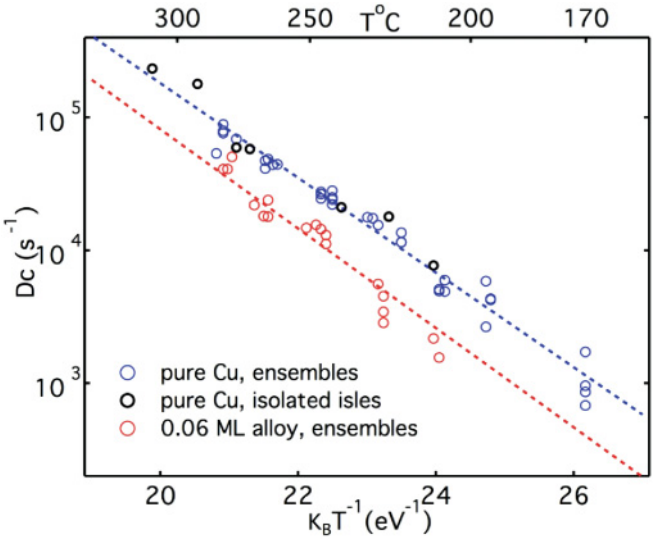

FIG. 9. (Color online) Values of Dc^{∞} versus temperature for the pure Cu(001) surface (blue) and the 0.06 ± 0.03-ML Pd alloy (red). Values from isolated island decays [Fig. 5(b)] are shown in black along with data from decay of island groups. Note that Dc^{∞} has been shortened simply to Dc on the vertical axis.

analysis of the temperature dependence of island decay rates. Instead, we estimate the change in the activation barrier versus Pd concentration using the approximation $\Delta E_a = -k_B T \ln(Dc^\infty / D_o c_o^\infty)$ at a fixed temperature ($T = 240\,^\circ$C). Figure 8(b) shows how E_a depends on the Pd concentration.

IV. DISCUSSION

How does buried Pd slow island ripening? It is possible that buried Pd (i) decreases the factor Dc^∞, e.g., by increasing the activation barrier, $E_a = E_f + E_m$, and/or (ii) decreases the step free energy (line tension), β.

Owing to the exponential dependence of the ripening rate on the activation barrier, E_a, we explore, first, how the buried Pd modifies E_a, since a small change $= k_B T = 40$ meV in E_m or E_f can cause a significant change $= 1/e$ in the product Dc^∞ and the island-ripening rate. By contrast, it is not likely that island ripening could be slowed by more than an order of magnitude (with 0.4-ML Pd) by a Pd-induced order-of-magnitude decrease in the step free energy.

To explain the ripening-slowing effect of buried Pd, we begin by exploring the mass transport mechanisms on the Cu(001) surface. We have used first-principles density-functional theory to calculate E_f and E_m for vacancies and adatoms on the pure Cu surface. Our results, consistent with other previous reports,[3,4,16–18] show that island ripening on the pure Cu surface is mediated by surface vacancies. In order to understand the slowing effect of Pd in the limit of dilute alloys ($\lesssim$0.20-ML Pd), we have explored the interaction of vacancies with isolated buried Pd atoms. We propose that dilute buried Pd slows surface diffusion primarily by impeding the migration of vacancies across terraces. In the next sections, we justify this conclusion.

A. Numerical methods

We conducted density-functional-theory (DFT) calculations of formation energies and diffusion barriers using the VASP DFT code[27–30] in the Perdew-Burke-Ernzerhof (PBE) version of the generalized gradient approximation (GGA),[31] with electron-nucleus interactions treated in the projector augmented wave (PAW) approximation.[32,33]

For vacancy diffusion we modeled the Cu(001) sample as a six-layer slab and for adatom diffusion used a five-layer slab instead. In both cases we isolated the diffusing species in a 4×4 supercell. Also in both cases, we fixed the atoms of the lower two slab layers in bulk Cu relative positions corresponding to the PBE optimal lattice parameter, 3.637 Å.

We sampled the surface Brillouin zone corresponding to our rather large supercell with a 4×4, equal-spaced set of k vectors, accelerated electronic relaxation by means of the Methfessel-Paxton Fermi-level-smearing method (width = 0.2 eV),[34] and corrected for the unphysical electric fields corresponding to periodic repetition of Cu slabs with different upper and lower surface atom arrangements, using the method of Neugebauer and Scheffler.[35] We used a plane-wave basis cutoff of 273 eV.

1. Adatom formation energy

To compute an Cu adatom formation energy, E_f^a, we applied

$$E_f^a = \{E^{\rm tot}(5-{\rm lyr\ slab}\ +\ {\rm adatom}) - [15\ E^{\rm tot}(5\text{-lyr slab}) + E^{\rm tot}(6\text{-lyr slab})]/16\}. \quad (5)$$

Physically, this approximate formula comes from imagining depositing 15 of the 16 Cu atoms of the upper layer of the six-layer slab, one each, onto 15 five-layer slabs. In the final state, there are then 16 five-layer slabs with a Cu adatom residing on each one. The formation energy is 1/16 the energy difference between the final and initial states.

2. Vacancy formation energy

To compute a vacancy formation energy, E_f^v, analogously, imagine removing a single Cu atom from each of 15 six-layer slabs and depositing them all on a single five-layer slab. The result is 16 six-layer slabs each possessing a surface vacancy. Accordingly, the vacancy formation energy is approximately

$$E_f^v = \{E^{\rm tot}(6\text{-lyr slab} - {\rm a\ surface\ atom}) - [15\ E^{\rm tot}(6\text{-lyr slab}) + E^{\rm tot}(5\text{-lyr slab})]/16\}.$$

3. Adatom and vacancy diffusion barriers on pure Cu(001)

Comparison of the energy of the PBE-optimized, five-layer slab with an adatom in a symmetric bridge site and in the equilibrium, fourfold hollow provided our estimate of the adatom hopping diffusion barrier on the pure Cu(001) surface. The barrier to concerted substitutional diffusion has been found by numerous groups to lie substantially higher.[36]

As illustrated in Fig. 10, we estimated the vacancy hopping diffusion barrier on the pure surface as the energy cost of displacing to a second-layer bridge site, an atom of the surface layer that initially lies adjacent to a surface layer vacancy. We also considered whether a concerted-substitutional vacancy diffusion mechanism (see Fig. 11) might be competitive. To do that, we used the nudged elastic band method,[37] with two replicas of the system between the initial state and the symmetric midpoint of the diffusion path.

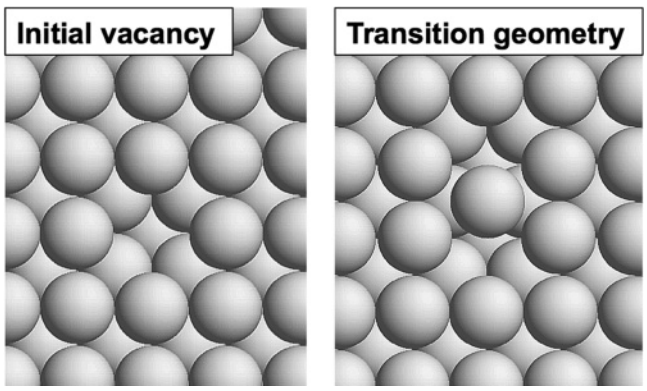

FIG. 10. (Left panel) A DFT optimized vacancy in the outer layer of a Cu(001) film. (Right panel) Midpoint of a vacancy diffusion event, amounting to displacement to a second-layer bridge site of a surface-layer atom initially adjacent to the vacancy.

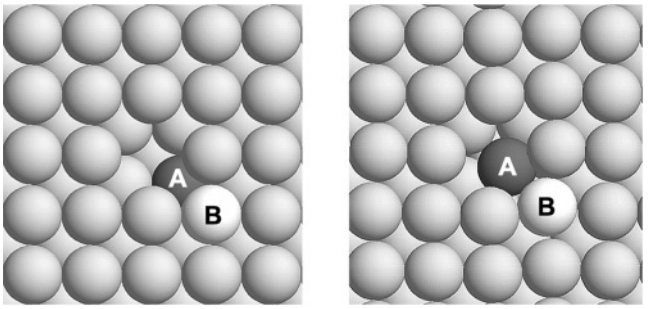

FIG. 11. (Left panel) A DFT optimized vacancy in the outer layer of a Cu(001) film. As the concerted diffusion event proceeds, the dark, second-layer atom, A, will rise, moving northwest, while the light atom, B, moves down to replace it. (Right panel) A geometry close to the transition state, whose energy is 0.63 eV higher than that of the structure shown in the left panel.

4. Vacancy diffusion past a second-layer Pd atom

We evaluated the diffusion barrier for vacancy displacement past a second-layer substitutional Pd atom as schematized in Fig. 12. In this case, because the Pd atom has a larger radius than a Cu, the barrier corresponds to bridge geometry asymmetric in the x direction and symmetric in the y direction, as illustrated in the right panel of the figure.

B. An attempt to reproduce the theoretical vacancy diffusion barrier on pure Cu(001) reported in Ref. 4

Klünker *et al.* reported in Ref. 4 an unexpectedly small DFT diffusion barrier for a vacancy on the pure Cu(001) surface, only 0.22 eV, based on a calculation using the PW91 version of the GGA. This value, they remarked, was already converged in a 3×3 supercell calculation for a four-layer Cu slab. Because 0.22 eV is only about half the barrier energy we computed, we hoped to identify the source of the difference by running VASP in the PAW approximation, with the same 3×3 supercell and slab thickness, a 4×4 equal spaced sample of the corresponding surface Brillouin zone, and a plane-wave basis cutoff of 273 eV. The result, however, a barrier energy of 0.41 eV, was reasonably close to what we had previously found with a larger unit cell, a thicker slab, and the PBE version of the GGA. Because of the poor agreement with the value of 0.22 eV published in Ref. 4, the question of why such a small barrier was found remains an open one.

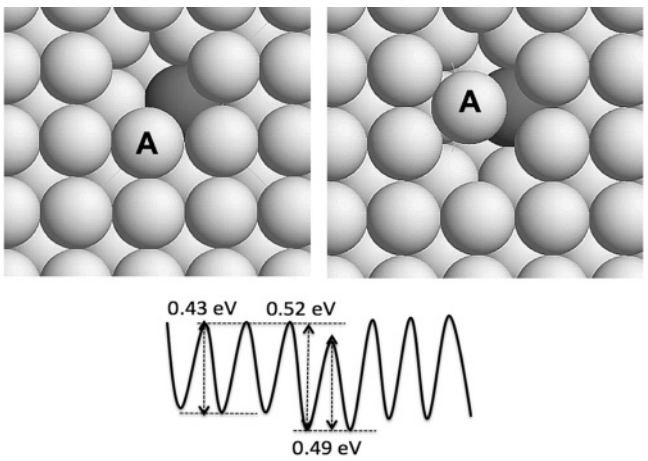

FIG. 12. (Left panel) A DFT optimized vacancy in the outer layer of a Cu(001) film, adjacent to a second-layer substitutional Pd impurity atom. The Cu atoms are light in color; the Pd atom is dark. Vacancy diffusion in the $-y$ direction amounts to displacement of the Cu atom, labeled A, in the $+y$ direction. (Right panel) Midpoint of atom A's minimum energy trajectory. Note that largely because the radius of a Pd atom exceeds that of a Cu by about 0.1 Å, A is displaced into contact with two Cu atoms on the left, in contrast to the symmetric transition geometry of Fig. 10. (Lower panel) A schematic representation of the effective potential for hopping past the Pd site.

C. Summary of DFT results

Our results are shown in Table I along with results from other previous studies obtained by DFT and the embedded atom method (EAM).

For vacancies on the clean Cu surface, we find a formation energy $E_f = 0.47$ eV, a migration barrier $E_m = 0.43$ eV, and $E_a = 0.90$ eV. For Cu adatoms, we find $E_f = 0.59$ eV, $E_m = 0.54$ eV, and $E_a = 1.13$ eV.

On alloy surfaces, we find that vacancies in the vicinity of a buried Pd atom experience an attraction (0.06 eV) to the (four) nearest-neighbor sites immediately above the buried Pd atom. With this attraction, the barrier to hop out of a nearest-neighbor site increases to 0.52 eV. The barrier to a diffusive hop between these nearest-neighbor sites is found to be 0.49 eV. A schematic of the barriers to vacancy hopping near a buried Pd atom is shown in Fig. 12 (lower panel).

D. Comparison of experiment and DFT results

Our DFT value $E_a = 0.90$ eV for vacancy-mediated ripening agrees quantitatively with $E_a = 0.83 \pm 0.03$ eV found in our experiments. By comparison, the 1.13-eV barrier calculated for adatom-mediated ripening is more than 0.2 eV larger. Activation barriers for concerted adatom and vacancy ripening are also predicted to be much larger than for vacancy-mediated ripening (see Ref. 36). Finally, the attachment-limited kinetics observed at smaller length scales and lower temperatures

TABLE I. Calculated adatom and vacancy formation energies and hopping barriers on the pure Cu(001) surface. Our density-functional-theory (DFT) results are given in bold.

	E_f (eV)	E_m (eV)	E_a (eV)
		Adatoms	
DFT	**0.59**	**0.54**	**1.13**
	0.48	0.52[3,18]	1.0[3]
EAM	0.71	0.50	1.21[3]
	0.66	0.49	1.15[38]
	0.71	0.48	1.19[39]
		Vacancies	
DFT	**0.47**	**0.43 (hop)**	**0.90**
		0.63 (concerted)	**1.1**
	0.22	0.42	0.64[3,18]
EAM	0.59	0.47	1.06[3]
	0.58	0.42	1.0[38]
	0.59	0.36	0.95[39]

by STM[3,4] is most easily understood as a consequence of vacancy-mediated diffusion. Therefore, we conclude surface vacancies mediate the ripening process on the pure Cu surface.

To model the effect of buried Pd on vacancy diffusion, we have created a kinetic Monte Carlo (KMC) simulation incorporating the calculated DFT barriers, Fig. 12 (lower panel), for the interaction of a vacancy with a buried Pd atom. In our simulation, Pd is incorporated into the subsurface layer on a randomly occupied $c(2 \times 2)$ lattice. A single isolated vacancy is incorporated into the surface layer. The vacancy performs a continuous-time random walk in the surface layer with hopping rates $\nu = \nu_\circ \exp(-E_m/k_BT)$ determined by the DFT barriers and a single attempt rate, $\nu_\circ$. We measure the average time, t, for the vacancy to migrate a fixed distance (33 lattice sites). The diffusion coefficient $D \propto 1/t$ gives a measure of the diffusion-slowing effect of a given Pd concentration.

Via our simulations, we find that D decreases with increasing Pd concentration, owing to the attraction of the vacancy to buried Pd. Figure 8(a) shows the Pd-coverage dependence of D/D_o obtained from the simulation. For Pd concentrations up to 0.2 ML, our model agrees reasonably with the experiment. Figure 8(b) shows the calculated change, ΔE_a, in the effective activation barrier for surface diffusion as a function of Pd coverage. As the Pd coverage increases, the calculated ΔE_a saturates at 0.49–0.43eV $= 0.06$ eV as the kinetics becomes dominated by the 0.49-eV barrier to hopping over buried Pd.

Note that the KMC simulation yields only the Pd-concentration dependence of D/D_o and does not account for possible changes in the vacancy concentration c. It is likely that the surface vacancy concentration, c, depends on the concentration, c_{Pd}, of buried Pd. Vacancies are attracted to buried Pd, and, hence, we expect that the vacancy formation energy should be smaller on alloyed surfaces. Using DFT calculations, we find that the formation energy (0.43 eV) for a vacancy at a site above an isolated Pd atom is ~40 meV smaller than on the pure Cu surface. Hence, it is likely that our model overestimates the slowing effect of Pd because it ignores the increase in vacancy concentration caused by the decrease in the formation energy. In our simulation we have a single vacancy diffusing on the Cu lattice. We mark its position at random times and then determine the average time, t, it takes to diffuse a fixed distance from this point. The tracer diffusion coefficient D is then proportional to $1/t$. To estimate the coverage dependence of Dc^∞ then requires us to scale $1/t$ with the average thermal occupancy of the starting position. This is simply $c = (1 - 4c_{\mathrm{Pd}}) \exp(-E_f^c/kT) + 4c_{\mathrm{Pd}} \exp(-E_f^{\mathrm{Pd}})$, where E_f^c is the formation energy of a vacancy on the clean surface, and E_f^{Pd} is the formation energy of a vacancy above a buried Pd. From our DFT results, $E_f^c - E_f^{\mathrm{Pd}} = 40$ meV. We have also plotted the Pd-coverage dependence of $Dc^\infty/D_oc_o^\infty$ in Fig. 8(a). For dilute Pd concentrations (<0.2 ML), the net effect of embedded Pd is to increase the effective ripening activation barrier as shown in Fig. 8(b). For Pd concentrations >0.20 ML, the change in the diffusion activation barrier, $\Delta E_a = \Delta E_f + \Delta E_m$, saturates at $-40 + 60 = 20$ meV, reflecting the competition between the decreasing E_f and increasing E_m with c_{Pd}. Clearly, the agreement between model and experiment is better when we consider only the effect of the buried Pd on D alone, which suggests that we have overestimated the effect of Pd on c.

Our model agrees with experiment for $c_{\mathrm{Pd}} < 0.2$ ML but deviates from it as c_{Pd} increases. Since our model accounts only for the interaction of a vacancy with a single isolated Pd atom, it accurately describes only the diffusion-slowing effect of Pd in dilute alloys where the majority of Pd sites are isolated. As Pd becomes more dense, it is plausible that there are configurations of adjacent Pd atoms that slow vacancy diffusion further. For example, in the case of Pb/Cu(111), the diffusion of Cu adatoms was found to be limited by a site-blocking effect involving two adjacent Pb atoms.[5] Exploring the potentials associated with the numerous atomic configurations in the case of more dense Pd is a subject for future work.

V. SUMMARY

We have shown that the rate of ripening of epitaxial Cu adatom islands on the Cu(001)-$c(2 \times 2)$-Pd surfaces decreases with increasing Pd concentration up to ~0.5-ML Pd. Previous measurements, and first-principles calculations, suggest that surface diffusion of Cu(001) is mediated by vacancies, not adatoms or clusters.[3,4,17] Our work independently confirms this conclusion: since the Pd in the surface alloy is primarily located one atomic layer below the surface, we propose that the buried Pd atoms impede the diffusion of surface vacancies. Our results suggest that a surface alloy of Pd-Cu may inhibit electromigration, as observed for Pd-Cu bulk alloys [6]. For example, extrapolating our experimental results to room temperature, we find that a 0.06-ML Pd surface alloy will inhibit surface-diffusion-limited electromigration rates by more than an order of magnitude.

ACKNOWLEDGMENTS

We thank B. S. Swartzentruber for insightful discussions and J. Hannon (IBM) for his image-analysis software. The work performed at Sandia was supported by the US Department of Energy, Office of Basic Energy Sciences, Division of Materials Science and Engineering. Sandia National Laboratories is a multiprogram laboratory operated by Sandia Corporation, a Lockheed-Martin Company, for the US Department of Energy under contract no. DE-AC04-94AL85000.

*ebussma@sandia.gov

[1] H. Brune, Surf. Sci. Rep. **31**, 125 (1998).
[2] M. Giesen, Prog. Surf. Sci. **68**, 1 (2001).
[3] J. B. Hannon, C. Klünker, M. Giesen, H. Ibach, N. C. Bartelt, and J. C. Hamilton, Phys. Rev. Lett. **79**, 2506 (1997).
[4] C. Klünker, J. B. Hannon, M. Giesen, H. Ibach, G. Boisvert, and L. J. Lewis, Phys. Rev. B **58**, R7556 (1998).
[5] M. L. Anderson, N. C. Bartelt, P. J. Feibelman, B. S. Swartzentruber, and G. L. Kellogg, Surf. Sci. **600**, 1901 (2006).
[6] W. L. Ling, N. C. Bartelt, K. Pohl, J. de la Figuera, R. Q. Hwang, and K. F. McCarty, Phys. Rev. Lett. **93**, 166101 (2004).

[7]C. K. Hu, R. Rosenberg, and K. Y. Lee, Appl. Phys. Lett. **74**, 2945 (1999).
[8]C. W. Park and R. W. Vook, Thin Solid Films **226**, 238 (1993).
[9]Z. Chen, N. Kioussis, K.-N. Tu, N. Ghoniem, and J.-M. Yang, Phys. Rev. Lett. **105**, 015703 (2010).
[10]G. W. Graham, P. J. Schmitz, and P. A. Thiel, Phys. Rev. B **41**, 3353 (1990).
[11]G. W. Anderson, K. O. Jensen, T. D. Pope, K. Griffiths, P. R. Norton, and P. J. Schultz, Phys. Rev. B **46**, 12880 (1992).
[12]A. R. Koymen, K. H. Lee, G. Yang, K. O. Jensen, and A. H. Weiss, Phys. Rev. B **48**, 2020 (1993).
[13]C. J. Barnes, E. A. T. Pitkanen, P. Kaukasoina, and M. Lindroos, Surf. Sci. **492**, 55 (2001).
[14]J. B. Hannon, J. Sun, K. Pohl, and G. L. Kellogg, Phys. Rev. Lett. **96**, 246103 (2006).
[15]J. Sun, J. B. Hannon, G. L. Kellogg, and K. Pohl, Phys. Rev. B **76**, 205414 (2007).
[16]R. van Gastel, E. Somfai, S. B. van Albada, W. van Saarloos, and J. W. M. Frenken, Phys. Rev. Lett. **86**, 1562 (2001).
[17]M. L. Grant, B. S. Swartzentruber, N. C. Bartelt, and J. B. Hannon, Phys. Rev. Lett. **86**, 4588 (2001).
[18]G. Boisvert and L. J. Lewis, Phys. Rev. B **56**, 7643 (1997).
[19]K. Barmak, C. Cabral, K. P. Rodbell, and J. M. E. Harper, J. Vac. Sci. Technol. B **24**, 2485 (2006).
[20]G. W. Anderson, T. D. Pope, K. O. Jensen, K. Griffiths, P. R. Norton, and P. J. Schultz, Phys. Rev. B **48**, 15283 (1993).
[21]C. Rottman and M. Wortis, Phys. Rev. B **24**, 6274 (1981).
[22]E. Bussmann, J. Sun, K. Pohl, and G. L. Kellogg, J. Phys. Condens. Matter **21**, 314106 (2009).
[23]M. A. V. Hove and S. Y. Tong, *Surface Crystallogrphy by LEED* (Springer-Verlag, Berlin, 1981).
[24]N. L. Petersen, Phys. Rev. **132**, 2471 (1963).
[25]M. Zinke-Allemang, L. C. Feldman, and M. H. Grabow, Surf. Sci. Rep. **16**, 377 (1992).
[26]C. Steimer, M. Giesen, L. Verheij, and H. Ibach, Phys. Rev. B **64**, 085416 (2001).
[27]G. Kresse and J. Hafner, Phys. Rev. B **47**, 558 (1993).
[28]G. Kresse and J. Hafner, Phys. Rev. B **49**, 14251 (1994).
[29]G. Kresse and J. Furthmuller, Comput. Mater. Sci. **6**, 15 (1993).
[30]G. Kresse and J. Furthmuller, Phys. Rev. B **54**, 11169 (1996).
[31]J. P. Perdew, K. Burke, and M. Ernzerhof, Phys. Rev. Lett. **77**, 3865 (1996).
[32]P. E. Blochl, Phys. Rev. B **50**, 17953 (1994).
[33]G. Kresse and D. Joubert, Phys. Rev. B **59**, 1758 (1999).
[34]M. Methfessel and A. T. Paxton, Phys. Rev. B **40**, 3616 (1989).
[35]J. Neugebauer and M. Scheffler, Phys. Rev. B **46**, 16067 (1992).
[36]Among GGA calculations, G. Boisvert and L. J. Lewis, Phys. Rev. B **56**, 7643 (1997), Table II reports a value of 0.96 eV, close to double the computed hopping barrier of 0.52 eV. H. Yildirim and T. S. Rahman, Phys. Rev. B **80**, 235413 (2009) obtained 0.79 eV compared to 0.53 eV for hopping. R. Pentcheva, Appl. Phys. A **80**, 971 (2005) reported 1.02 eV as against 0.49 eV for hopping. In a local density approximation calculation, C. M. Chang and C. M. Wei, Chinese J. Phys. **43**, 169 (2005), found a value of 0.94 eV for concerted diffusion and 0.64 eV for hopping.
[37]H. Jonson, G. Mills, and K. W. Jacobsen, in *Classical and Quantum Dynamics in Condensed Phase Simulations*, edited by B. J. Berne, G. Ciccotti, and D. F. Coker (World Scientific, Singapore, 1998).
[38]S. V. Eremeev, A. G. Lipnitskii, A. I. Potekaev, and E. V. Chulkov, Russ. Phys. J. **40**, 584 (1996).
[39]M. Karimi, T. Tomkowski, G. Vidali, and O. Biham, Phys. Rev. B **52**, 5364 (1995).